Design and characterization of whispering-gallery spiral waveguides

Tong Chen, Hansuek Lee, and Kerry J. Vahala*

T. J. Watson Laboratory of Applied Physics, California Institute of Technology, Pasadena, California, 91125, USA

*vahala@caltech.edu

Abstract: Whispering gallery delay lines have demonstrated record propagation length on a silicon chip and can provide a way to transfer certain applications of optical fiber to wafer-based systems. Their design and fabrication requires careful control of waveguide curvature and etching conditions to minimize connection losses between elements of the delay line. Moreover, loss characterization based on optical backscatter requires normalization to account for the impact of curvature on backscatter rate. In this paper we provide details on design of Archimedean whispering-gallery spiral waveguides, their coupling into cascaded structures, as well as optical loss characterization by optical backscatter reflectometry.

OCIS codes: (230.7390) Waveguides, planar; (220.0220) Optical design and fabrication.

References and links

1. H. Lee, T. Chen, J. Li, O. Painter, and K. J. Vahala, "Chemically etched ultrahigh-Q wedge-resonator on a silicon chip," Nat. Photonics **6**, 369–373 (2012).
2. H. Lee, T. Chen, J. Li, O. Painter, and K. J. Vahala, "Ultra-low-loss optical delay line on a silicon chip," Nat. Commun. **3**, 867 (2012).
3. K. Takada, H. Yamada, Y. Hida, Y. Ohmori, and S. Mitachi, "Rayleigh backscattering measurement of 10m long silica-based waveguides," Electron. Lett. **32**, 1665–1667 (1996).
4. J. F. Bauters, M. Heck, D. John, D. Dai, M. Tien, J. S. Barton, A. Leinse, R. G. Heideman, D. J. Blumenthal, and J. E. Bowers, "Ultra-low-loss high-aspect-ratio Si_3N_4 waveguides," Opt. Express **19**, 3163–3174 (2011).
5. B. Soller, D. Gifford, M. Wolfe, and M. Froggatt, "High resolution optical frequency domain reflectometry for characterization of components and assemblies," Opt. Express **13**, 666–674 (2005).
6. T. Chen, H. Lee, J. Li, and K. J. Vahala, "A general design algorithm for low optical loss adiabatic connections in waveguides," Opt. Express **20**, 22819–22829 (2012).
7. R. Adar, M. Serbin, and V. Mizrahi, "Less than 1 dB per meter propagation loss of silica waveguides measured using a ring resonator," J. Lightwave Technol. **12**, 1369–1372 (1994).
8. M. Cai, O. Painter, and K. J. Vahala, "Observation of critical coupling in a fiber taper to silica-microsphere whispering gallery mode system," Phys. Rev. Lett. **85**, 74–77 (2000).
9. S. M. Splillane, T. J. Kippenberg, O. J. Painter, and K. J. Vahala, "Ideality in a fiber-taper-coupled microresonator system for application to cavity quantum electrodynamics," Phys. Rev. Lett. **91**, 043902 (2003).
10. H. Lee, M. Suh, T. Chen, J. Li, S. Diddams, and K. J. Vahala, "Spiral resonators for on-chip laser frequency stabilization," Nat. Commun. **4**, 2468 (2013).
11. T. Chen, H. Lee, and K. J. Vahala, "Thermal stress in silica-on-silicon disk resonators," Appl. Phys. Lett. **102**, 031113 (2013).

1. Introduction

Recently, a method of fabricating ultra-high-Q resonators in silica on silicon wafers was reported [1]. Because the processing of these structures uses conventional lithography and etching, there is a high level of size control possible. As an important extension of the process,

#200514 - $15.00 USD Received 5 Nov 2013; revised 27 Jan 2014; accepted 10 Feb 2014; published 27 Feb 2014

whispering-gallery waveguides were later developed [2]. These waveguides are, so far, as long as 27 meters and exhibit optical waveguide loss as low as $0.05 dB/m$ [2]. This new waveguide provides a technology for implementing time delay on a chip that has only been possible before using optical fiber. In this paper, the design and fabrication of these whispering-gallery delay lines as well as their loss characterization is described in further detail. Design of Archimedean spirals, their interconnection both as interleaved spirals and in cascade format, and derivation of the backscatter renormalization equation introduced in [2] are described. In addition, new characterization measurements to infer the insertion loss of adiabatic coupling of interleaved spirals are presented. The paper is organized as follows. In section 2 spiral design principles and example implementations are described. The approach here can be generalized for design of new geometries and delay-line layouts. In section 3 a discussion of loss characterization using backscatter reflectometer methods is provided. Also, the correction formula to convert backscatter data into optical loss is derived and used to analyze several different spiral geometries. Finally, in section 4 a discussion of buffer pattern design is provided. These buffer patterns are required to maintain proper etch uniformity over the wafer.

2. Archimedean spiral waveguide design and characterization

As conventional whispering-gallery mode resonators [1], whispering-gallery waveguides confine and guide optical modes along the curved surface defined by the exterior edge of the waveguide as shown in Fig. 1(c) inset. Therefore, to both maximize length and to also maintain a continuously curved surface without the rapid change of curvature, the waveguide delay lines are typically designed with multiple individual Archimedean spirals that are either interleaved or connected together [2]. Interleaved Archimedean spirals are connected by an S-bend connection waveguide in the center to provide adiabatic change of mode location between clockwise and counterclockwise spiral waveguides (Fig. 1(b)). In addition to the waveguides, themselves, a buffer pattern is also introduced to improve etch uniformity across the wafer. The buffer pattern, consisting of parallel lines of oxide stripes, creates a uniform loading for the dry etchant used to etch the silicon. Figure 1(a) shows an example of a waveguide design featuring all of these design elements. Specifically, in this cascaded design there are pairs of interleaved Archimedean spirals that provide input/output waveguides. Each pair is connected to a neighboring pair to create the cascade for greater overall length. Finally, S-bend waveguides are visible and expanded upon in Fig. 1(b). The buffer pattern is also visible in Fig. 1(a). In addition to the linear buffering, there are also buffer features added near the S-bend structure (see Fig. 1(b)) to control the dry-etching rate.

The process used to fabricate these waveguides is described in detail in [2], however, briefly, it proceeds in three steps: lithography, wet etch of a thermal silica layer, and then dry etch of the silicon to undercut the silica. A cross section of a portion of the Archimedean spiral is shown in Fig. 1(c). Besides the width of the waveguide, the undercut of the silicon during the dry etch process must be carefully controlled. Also, a feature of the wet etch step is a wedge-shaped profile in the oxide. The angle of this wedge can be controlled in the process and larger wedge angles have been shown to be beneficial for reduced optical loss [1].

2.1. Archimedean spirals

Archimedean spirals are frequently used in chip waveguides [2–4] since they provide the optimal area utilization. A typical design includes two, interleaved Archimedean-shaped spirals, one that brings light from the exterior to the interior and the other that returns the light to the

#200514 - $15.00 USD Received 5 Nov 2013; revised 27 Jan 2014; accepted 10 Feb 2014; published 27 Feb 2014

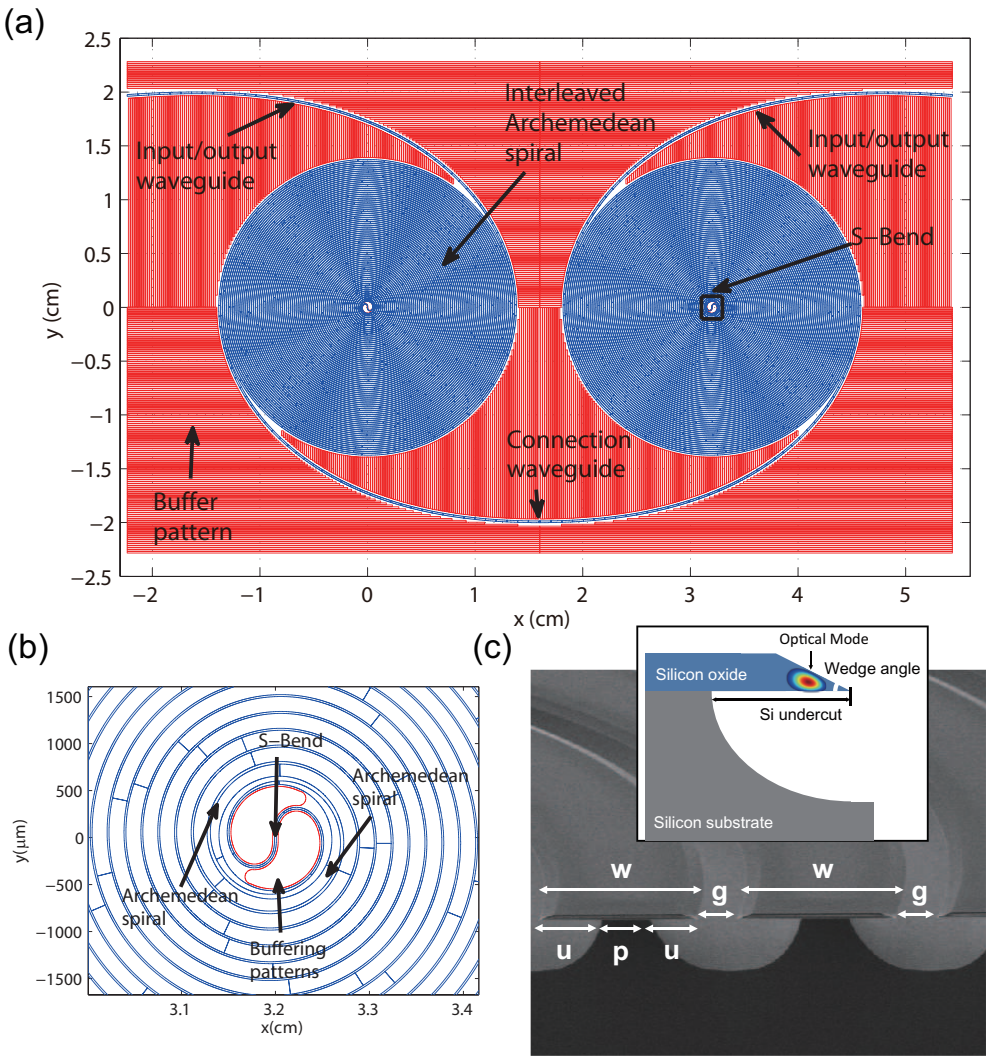

Fig. 1. An example of the spiral waveguide design. **(a)** A MATLAB generated spiral waveguide design consisting of two, interleaved pairs of Archimedean spirals. The surrounding red stripes are buffer patterns to provide etch uniformity. **(b)** A zoom-in view of the center-of-spiral waveguide pattern. The red patterns in the center are buffer patterns to control the etch loading near the S-bend connection. **(c)** An SEM image showing a cross section of the Archimedean part of spiral waveguide. w is the width of the waveguides; g is the separation between two neighbouring waveguides; u is the silicon undercut; and p is the width of the supporting silicon pillar. Inset shows a schematic of the spiral waveguide cross section.

exterior. In Cartesian coordinates, the spirals can be parameterized by the angle θ as

$$\begin{cases} x_c(\theta) = (R_0 + A \cdot \theta) \cdot \sin(\theta) \\ y_c(\theta) = (R_0 + A \cdot \theta) \cdot \cos(\theta) \end{cases} \tag{1}$$

where parameter R_0 controls the starting position of the spiral and parameter A determines the distance between successive turnings. Since this function only defines an isolated curve,

#200514 - $15.00 USD Received 5 Nov 2013; revised 27 Jan 2014; accepted 10 Feb 2014; published 27 Feb 2014

two parallel curves ((x_{in},y_{in}), (x_{out},y_{out}))are required (inner and outer boundaries) to define a waveguide.

$$\begin{cases} x_{in}(\theta) = x_c(\theta) - n_x(\theta)\cdot w_{in}(\theta) \\ y_{in}(\theta) = y_c(\theta) - n_y(\theta)\cdot w_{in}(\theta) \end{cases} \tag{2}$$

$$\begin{cases} x_{out}(\theta) = x_c(\theta) + n_x(\theta)\cdot w_{out}(\theta) \\ y_{out}(\theta) = y_c(\theta) + n_y(\theta)\cdot w_{out}(\theta) \end{cases} \tag{3}$$

where $(n_x(\theta), n_y(\theta))$ defines the normal vector of the curve in Eq.(1) and $w(\theta) = w_{in}(\theta) + w_{out}(\theta)$ gives the width of waveguide.

The Archimedean part of a spiral waveguide (i.e., non S-bend part) typically has a constant width and thus is characterized by three parameters: the starting size of the spiral (R_0), the width of waveguide (w) and the separation between two neighbouring waveguides (g). w and g determine the parameter A in the Archimedean spiral through the expression $A = \frac{w+g}{\pi}$ (see Fig. 1(c)).

To achieve longer waveguide length in a given footprint, narrow waveguides are favorable.

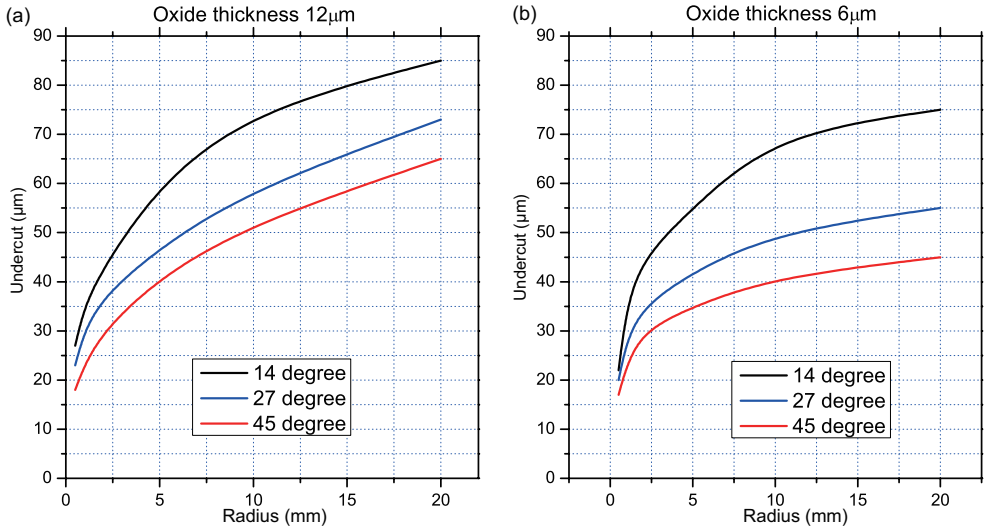

Fig. 2. Desired silicon undercut to attain a waveguide loss less than $0.1\,dB/m$ for oxide thicknesses $12\,\mu m$ (panel (a)) and $6\,\mu m$ (panel (b)) and wedge angles 14°, 27°, 45°.

Yet, the minimum width of the waveguide (w) is determined by the required undercut (u) and etching uniformity (see Fig. 1(c)). Concerning the required undercut, ultra-low-loss operation requires sufficient silicon undercut to avoid interaction between the lightwave in the silica with the silicon substrate. Figure 2 summarizes finite element modeling to determine conditions necessary to limit silicon-related waveguide loss to less than $0.1\,dB/m$. Besides the radius of the waveguide, both the waveguide thickness and the silica wedge angle are varied in the plots. Thicker oxides with larger wedge angles require less undercutting of the silica to maintain low loss. Also, larger undercut is required for waveguides having larger radius of curvature. Using an $8-10\,\mu m$ thick oxide with a 27 degree wedge angle, the maximum radius of curvature will occur at connections in cascaded designs (see Fig. 1(a) and Fig. 4(b)). In the largest designs to

#200514 - $15.00 USD Received 5 Nov 2013; revised 27 Jan 2014; accepted 10 Feb 2014; published 27 Feb 2014

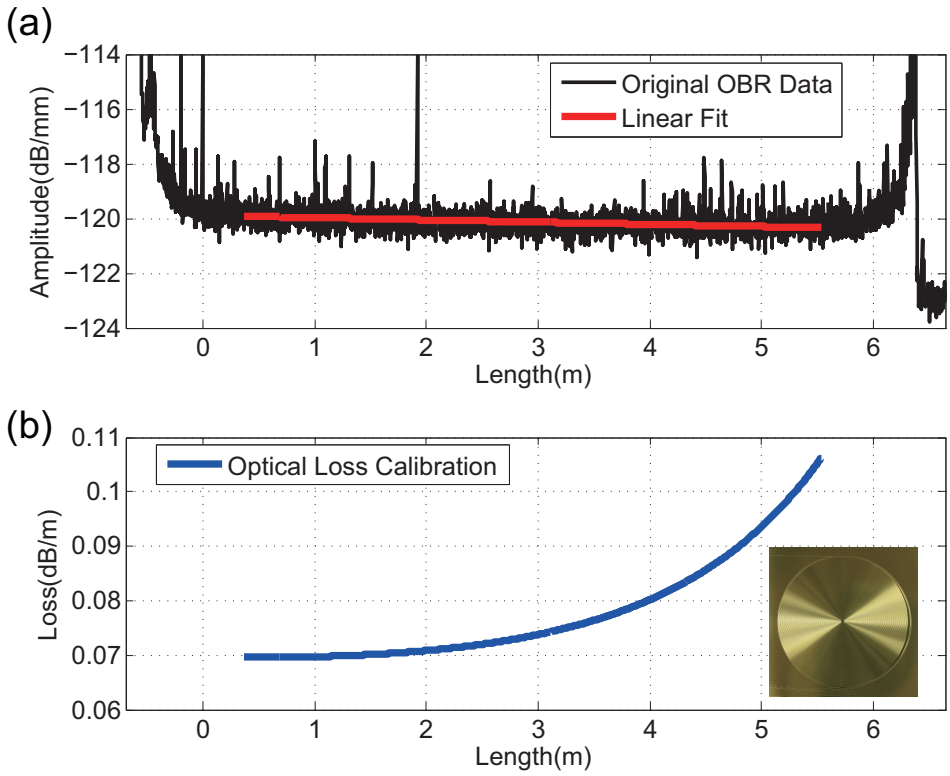

Fig. 3. Measurement and calibration of spiral waveguide attenuation using optical backscatter reflectometer (OBR) data. The simple linear fitting of optical backscatter reflectometer data in panel (a) gives an underestimated $0.05\,dB/m$ loss. In contrast, panel (b) shows the more accurate local attenuation rate calibrated based on Eq. (7). Inset of panel (b) is a photograph of a one-way spiral with a path length of approximately $7\,m$.

date, the curvature radii of these connections can reach $20\,cm$ thereby requiring over $70\,\mu m$ of silicon undercut. Also, etch non-uniformity in the range of $5-10\%$ requires that this undercut be increased somewhat. Therefore, assuming a support pillar width of $20\,\mu m$, the minimum required width of the waveguide is $160\,\mu m$.

2.2. Characterization of "one-way" spiral waveguides

To characterize the waveguide loss, we first fabricate a "one-way" spiral, which is a single, counter-clockwise Archimedean spiral that terminates near the center of the spiral (inset of Fig 3(b)) [2]. The spiral shown has a diameter of $4.3\,cm$ with a physical path length of approximately $7\,m$. An optical backscatter reflectometer (Luna OBR 4400) is used to characterize waveguide attenuation [5]. The data in Fig 3(a) show an approximately linear decrease (on the log scale) over nearly the full 7 m of the spiral path. The inferred loss rate from this data via a linear regression is $(0.05\pm0.01)\,dB/m$ and provides a lower bound on the waveguide attenuation rate. To calibrate this estimation, the impact of the varying backscatter signal caused by the changing radius of curvature is accounted for in the measurement. For this calibration, we

#200514 - $15.00 USD Received 5 Nov 2013; revised 27 Jan 2014; accepted 10 Feb 2014; published 27 Feb 2014

begin with a simple power attenuation equation

$$\frac{dP(z)}{dz} = -\alpha(z)P(z) \tag{4}$$

where $P(z)$ is the optical power at location z and $\alpha(z)$ the local waveguide attenuation. By assuming that backscatter strength is proportional to attenuation with coefficient $C(z)$, we have

$$\beta(z) = C(z)\alpha(z) \tag{5}$$

where $\beta(z)$ is the local backscattering rate. This assumption requires that waveguides are scattering-loss limited as opposed to absorptive-loss limited, and bending loss is minimal for a typical structure with radius greater than $100\,\mu m$. This property was verified for the waveguides of this study [1]. Since the detected backscattering signal $\big(B(z)\big)$ is further attenuated during its back-propagation, we have

$$B(z) = e^{-\int_0^z \alpha(s)ds}\beta(z)P(z) \tag{6}$$

By differentiating Eq.(6), a simple differential equation relates the measured backscatter power, $B(z)$, to local waveguide attenuation, $\alpha(z)$. The equation is given by,

$$\frac{1}{B(z)}\frac{dB(z)}{dz} = -\Big[2\alpha(z) - \frac{1}{\alpha(z)}\frac{d\alpha(z)}{dz}\Big] \tag{7}$$

This equation shows that when the attenuation rate is changing with distance (in the present case on account of the slowly changing radius of the waveguide), there is a slight correction to the loss as inferred from the backscatter rate. Inward spiraling waves produce a backscatter signal that attenuates more slowly on account of this term, while outward spiraling waves appear to decay more quickly. Figure 3 shows the impact of the correction term in Eq. (7). The simple linear fitting in Fig. 3(a) gives an underestimated $0.05\,dB/m$ loss. In contrast, a more precise local attenuation rate can be calculated using Eq. (7) as shown in Fig. 3(b) with about $0.07\,dB/m$ loss at the outside of the spiral. It should be noted that a minimum, corrected optical loss of $0.05\,dB/m$ has been measured on another waveguide [2].

2.3. Characterization of "two-way" spiral waveguides

A functional spiral waveguide requires both input and output (a "two-way" spiral). Figure 4(b) shows such a device with four "two-way" spirals cascaded on a single wafer to create a $27\,m$ (physical length) waveguide. Each spiral features inward and outward, interlaced Archimedean-shaped waveguides that are connected at the spiral center by an S-bend described in Sec. 3. The linear fit of the backscattering signal of each section of waveguide (see red lines in Fig. 4(a)) must be recalibrated on account of the mechanism described in Sec. 2.2. Specifically, the optical mode of waveguide in smaller radii sections of the waveguide experiences stronger surface scattering and will thus generate stronger backscattering signal with the same power. Therefore, the more rapid decrease of the curvature radius in the inward Archimedean spiral leads to underestimation of its attenuation and even negative apparent attenuation rate (due to the positive slope of backscattering signal), whereas in the outward Archimedean spiral the attenuation is overestimated. The local attenuation rate should be calibrated based on Eq. (7). Such an example is shown in Fig. 4(c) for the third spiral in Fig. 4(b) (lower right in the figure). At the outer part of the spiral, the attention rate is less than $0.1\,dB$ and this value increases to over $0.2\,dB$ towards the center of the spiral as the radius decreases. The increase of the loss is due to the higher surface scattering loss of the smaller curvature radius waveguides.

#200514 - $15.00 USD Received 5 Nov 2013; revised 27 Jan 2014; accepted 10 Feb 2014; published 27 Feb 2014

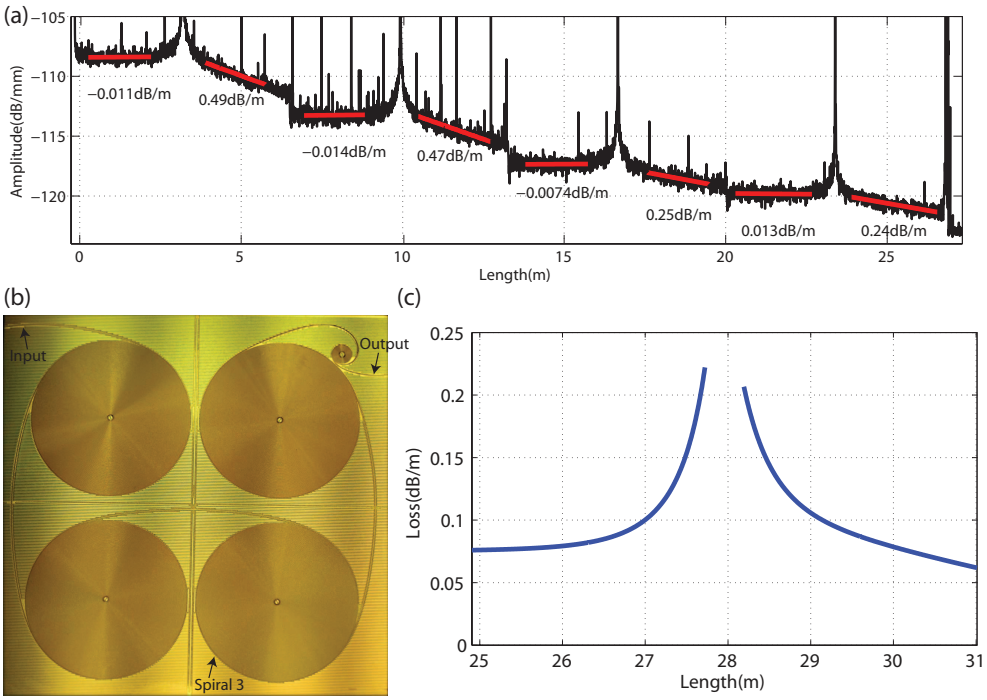

Fig. 4. Backscatter reflectometer study of optical waveguide loss in a cascaded spiral waveguide structure having length in excess of 27 meters. **(a)** Optical backscatter reflectometer data measured by coupling light at the upper left input waveguide in panel (b). The red lines show the corresponding uncorrected waveguide loss rates that do not account for variation of backscattering using Eq. (7). **(b)** Photograph of a cascaded, four-spiral waveguide having a physical path length of $27\,m$. Each spiral is approximately $4\,cm$ in diameter (Originally appearing in [2]). Input and output coupling occur in the upper left and upper right sides of the chip. **(c)** The calibrated local attenuation rate in spiral 3 of Fig. 4(b) (see spiral in lower right) calibrated using Eq. (7). This should be compared to the uncorrected, simple linear fit (red line) in Fig. 4(a).

As described in [2], the analysis of waveguide attenuation in individual two-way spirals of Fig. 4(b) may be performed by plotting the ratio of out-going to in-going backscatter strength at equidistant points from the spiral center. Since two equidistant points have the same radius and therefore the same backscattering rate, the ratio of their backscattering strengths gives the ratio of the optical powers. The slope of the resulting linear fit gives average loss for the waveguide, while the intercept gives an insertion loss for the S-bend adiabatic coupler [2].

3. Design and characterization of connections between interleaved Archimedean spiral waveguides

S-bend connection occurs when two interleaved Archimedean spirals (one clockwise and one counter clockwise) must be joined near the center of either spiral. In previous research [3, 4], the S-bend waveguide paths have been constructed from sinusoidal curves, ellipses or other families of curves that are not necessarily the optimal choice. Using the algorithm described in [6], an optimal S-bend can be designed so as to minimize excitation of higher-order modes and smoothly connect to the Archimedean spirals. Schematics of S-bends are presented in

#200514 - $15.00 USD Received 5 Nov 2013; revised 27 Jan 2014; accepted 10 Feb 2014; published 27 Feb 2014

Figs. 1(a) and 1(b) and a micrograph of a fabricated S-bend waveguide is shown in Fig. 5(a).

S-bend connection waveguides are defined by the R_0 and A of the outside Archimedean spiral to which it connects as well as the angle at the connection point [6]. As discussed in Sec. 2.1, the parameter A is determined by the width of the waveguide (w) and the separation between adjacent waveguides (g). R_0 and the angle at the point of connection are therefore adjusted as free parameters to match the desired size of the S-bend connection and to maintain continuity of curvature between the S-bend and the Archimedean waveguide.

3.1. Tapering of waveguide in the S-connection

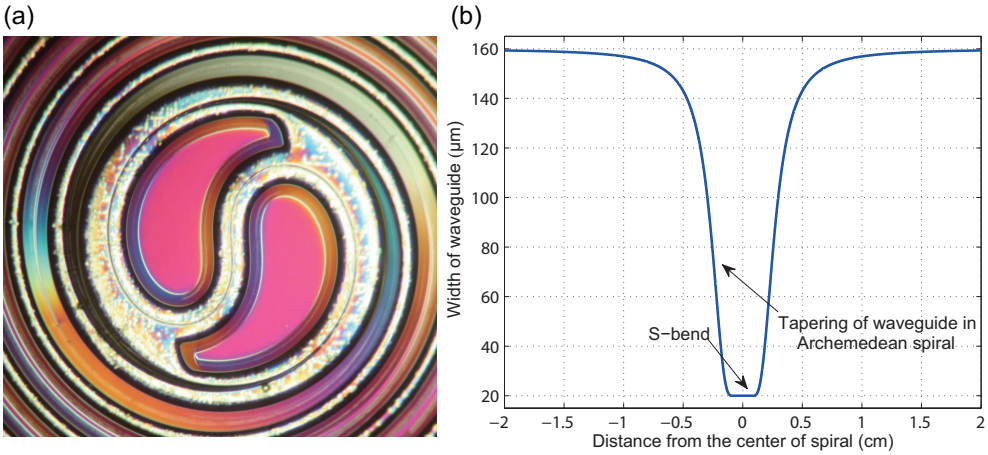

Fig. 5. An example of the S-bend waveguide connection used to connect clockwise and counter-clockwise Archimedean spiral waveguides. **(a)** A microscope image of of the S-bend connection. Also apparent in the image is tapering of the Archimedean spiral waveguide width as it approaches the S-bend connection near the center of spiral. **(b)** A plot shows the width of the Archimedean spiral waveguide in the tapering region (see discussion in Sec. 3.1).

A narrow waveguide ($10-20\,\mu m$) is desirable in the S-bend region to avoid intermode coupling [6], whereas the Archimedean part of the spiral requires a wide waveguide width ($\sim 150\,\mu m$) to enable sufficient undercut upon dry etching. Therefore, to achieve a smooth connection between the outside Archimedean spiral and the inner S-bend connection, the width of the waveguide must be varied adiabatically. Mathematically, we are looking for a function $f(x)$ such as

$$\begin{aligned} f(0) &= w_1 \\ f(x) &\to w_2 \qquad \text{as } x \to \infty \\ f'(0) &= f''(0) = 0 \end{aligned} \tag{8}$$

where w_1 and w_2 are the desired waveguide widths of the S-bend and Archimedean spiral. The third condition in Eq.(8) will guarantee that the tapering will not disturb the continuity property of the waveguide's tangent angle and curvature at the connection. A family of Hill functions satisfies these requirements

$$H_{n,d}(x) = \frac{(\frac{x}{d})^n}{1+(\frac{x}{d})^n} \tag{9}$$

#200514 - $15.00 USD Received 5 Nov 2013; revised 27 Jan 2014; accepted 10 Feb 2014; published 27 Feb 2014

where n and d are controllable parameters and $n \geq 3$ is required for the third condition in Eq.(8). Specifically, n defines the steepness the tapering function and d gives the scale of the tapering region. The waveguide width in the Archimedean part of the spiral (parameterized as in Eq. (1)) is then given by

$$w(\theta) = w_1 + (w_2 - w_1) \cdot \frac{(\frac{\theta}{d})^n}{1 + (\frac{\theta}{d})^n} \tag{10}$$

Figure 5 illustrates the tapering waveguide near the center of the spiral. The designed waveguide width of the S-bend connection region is $20\,\mu m$ whereas the Archimedean part of the spiral has a width of $160\,\mu m$. A Hill function with $n = 3$ and $d = \pi$ is employed here to taper the waveguide.

Using the insertion loss approach described in Sec. 3.2, we measure the insertion loss of S-bend connections with various tapering rates. For an S-bend connection with $A = 500\,\mu m$, we varied the d parameter in the Hill function from (c.f. Eq.(10)) 0.5π to π. The data in Fig. 6 show that a slower tapering rate (larger value of d) tends to provide less optical insertion loss. This can be attributed to the adiabatic requirement in varying the waveguide width.

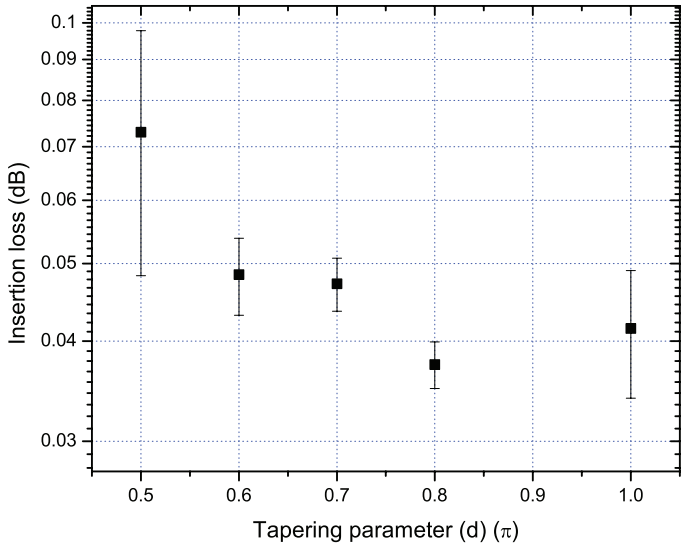

Fig. 6. Loss measurement results for an S-bend connection with various tapering rates (d). The structure measured has $A = 500\,\mu m$, while the d parameter in the Hill function is varied from 0.5π to π. The data show an average loss value measured from $3-5$ devices, and the error bars gives the standard deviation. The fluctuation mainly comes from fabrication imperfection.

3.2. Connection of cascaded Archimedean spirals

Besides the interleaved Archimedean spirals and S-bend connection, a complete design of spiral waveguides also requires for the connection waveguide between cascaded spirals as well as the waveguide path guiding the lightwave in and out of the spiral waveguide (see Fig. 1). As was true for the S-bend connection, the method of [6] can be applied readily to establish the connection between cascaded spirals. Figure 7 provides an illustration of a typical design. Focusing on the red, arc segment, one endpoint occurs at the Archimedean spiral (see right

#200514 - $15.00 USD Received 5 Nov 2013; revised 27 Jan 2014; accepted 10 Feb 2014; published 27 Feb 2014

side in Fig. 7) and has position (x_0, y_0), tangential angle θ_0 and curvature κ_0. The mirror-image segment (in black) has an endpoint (x_1, y_1) with tangential angle θ_1 and curvature κ_1 where (by symmetry) $\theta_1 = \pi$. We consider a family of curves with curvature given in terms of a cubic polynomial of arc length "s" [6].

$$\kappa(s) = a_0 + a_1 s + a_2 s^2 + a_3 s^3 . \tag{11}$$

The coefficients of the polynomial (a_i) and connection waveguide length s_1 are determined by matching the endpoint positions, endpoint tangents and the curvature between start and end points.

$$\begin{cases} a_0 = \kappa_0 \\ \theta_1 = \theta_0 + \int_0^{s_1} \kappa(s) ds = \theta_0 + \int_0^{s_1} a_0 + a_1 s + a_2 s^2 + a_3 s^3 \, ds \\ \kappa_1 = a_0 + a_1 s + a_2 s^2 + a_3 s^3 |_{s=s_1} \\ (x_1, iy_1) = (x_0, iy_0) + \int_0^{s_1} \exp(i\theta(s)) ds \end{cases} \tag{12}$$

By solving Eq. (12), a curve for the adiabatic connection is successfully defined via a_i and s_1 as shown in Fig. 7.

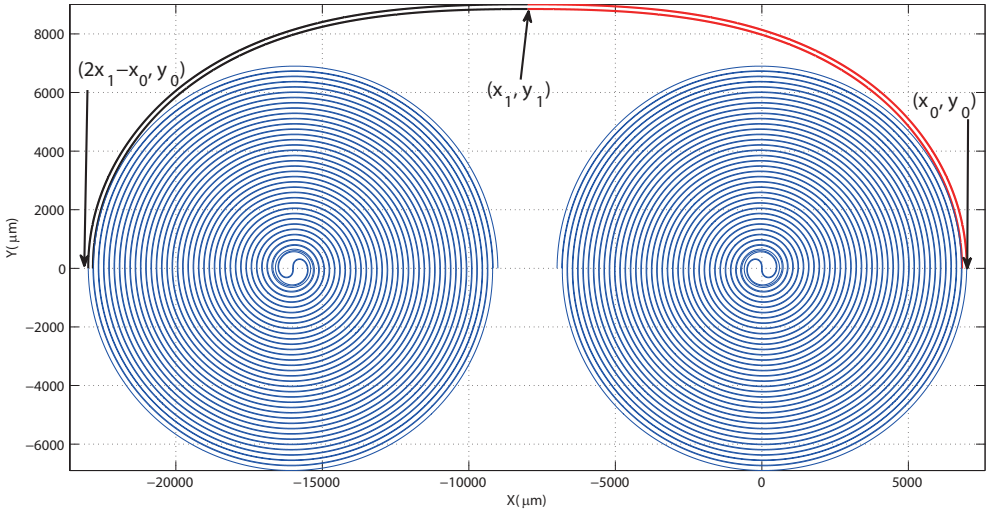

Fig. 7. An example showing connection of cascaded spirals. The blue curves outline two identical individual spirals to be connected. The red waveguide starts at (x_0, y_0) and ends at (x_1, y_1). The black curve starts at $(2x_1 - x_0, y_0)$ and ends at (x_1, y_1).

3.3. Characterization of S-bend connection loss

Measurement of S-bend connection loss in waveguides is complicated by the insertion loss associated with coupling light into the waveguide. Resonator Q characterization provides one of the most reliable methods [7]. Therefore, as an additional check of the S-bend insertion loss (beyond the method described in Sec. 3.1), we also employed closed-loop resonators consisting of two couplers (see micrograph of a typical, double-S-bend resonator in Fig. 8(a)). In these devices the dominant source of round trip loss is provided by the S-bend connection (*i.e.*, not the waveguide loss). As a result the Q factor of the resonators is dominated by the insertion loss of the two, S-bend connections. The resonators consisting of two S-bend connection are fabricated via the same process as the spiral waveguide [2]. The spectral measurement of Q factor was used

#200514 - $15.00 USD Received 5 Nov 2013; revised 27 Jan 2014; accepted 10 Feb 2014; published 27 Feb 2014

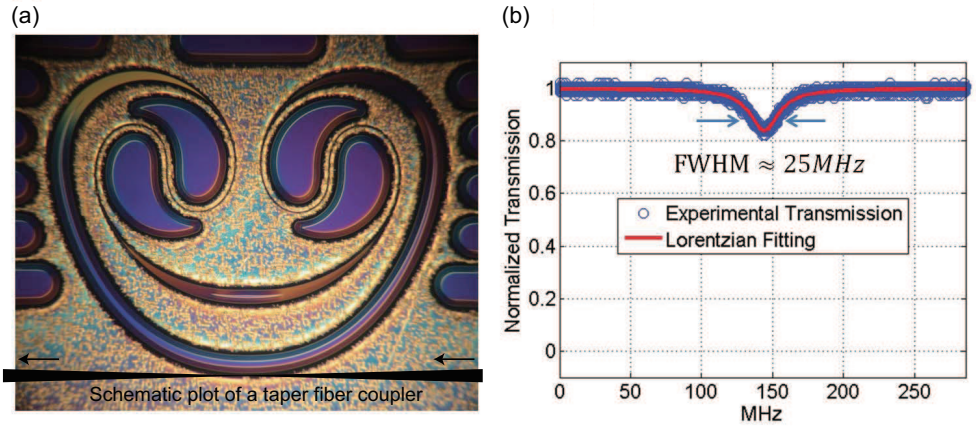

Fig. 8. **(a)** An optical micrograph of a resonator formed from two S-bend connections with schematic plot of a taper fiber coupler. This resonator has a round trip length of $1.5\,cm$. Buffer patterns are introduced to improve the etching uniformity. **(b)** A spectral scan for the resonator in panel (a) having of a Q factor of 8×10^6.

and a typical spectrum for the resonator of Fig. 8(a) is provided in Fig. 8(b). The coupling to the resonator used a fiber taper positioned at the lower waveguide edge of the resonator [8, 9]. The Q factor is as high as 8×10^6 which implies less than $0.025\,dB$ loss provided by each of the S-bend connectors. The optical performance of various S-bend structures having different size parameters A is summarized in Fig. 9. Briefly, for a large ($A > 200\,\mu m$) S-bend connection the measured loss is higher because the length of the higher-loss, S-bend waveguide increases with increasing A. The very small S-bend ($A < 100\,\mu m$) designs are, however, not satisfactory either. Here, the rapid change of curvature brings inter-mode coupling and consequently higher optical loss [6]. The optimal value of size parameter A was found to be between $100\,\mu m$ and $200\,\mu m$ and to provide less than $0.02\,dB$ insertion loss. This optimum design of S-bend connection was applied on spiral resonators having $1.2\,m$ path length, which showed 140 million Q [10].

4. Buffer patterns

In most portions of the spiral, the Archimedean topology provides the uniform loading upon the xenon difluoride etching. Nevertheless, since the cleaved sample typically has a rectangular shape and the waveguide pattern only covers part of the entire chip, the waveguide pattern will be surrounded by exposed silicon upon oxide etching. The etching rate at the outside of the pattern which requires larger undercut as shown on Fig. 2 will consequently be slower than at the center and may fail to create enough undercut. Meanwhile, the S-bend connection also exhibits non-uniform loading during dry etching and deserves special treatment. To address these issues, buffering patterns are introduced to improve the etching uniformity across the entire chip by maintaining uniform loading in the etching. This can be achieved by keeping the local ratio between the area of exposed silicon and silica mask the same over the chip. For the spiral waveguide region of the chip, this ratio is determined by waveguide width (w) and the gap between adjacent waveguides (g). Therefore, parallel rectangular patterns with width ($2 \times w$) and gap ($2 \times g$) are added to the area surrounding the waveguide (see Fig. 1(a)).

#200514 - $15.00 USD Received 5 Nov 2013; revised 27 Jan 2014; accepted 10 Feb 2014; published 27 Feb 2014

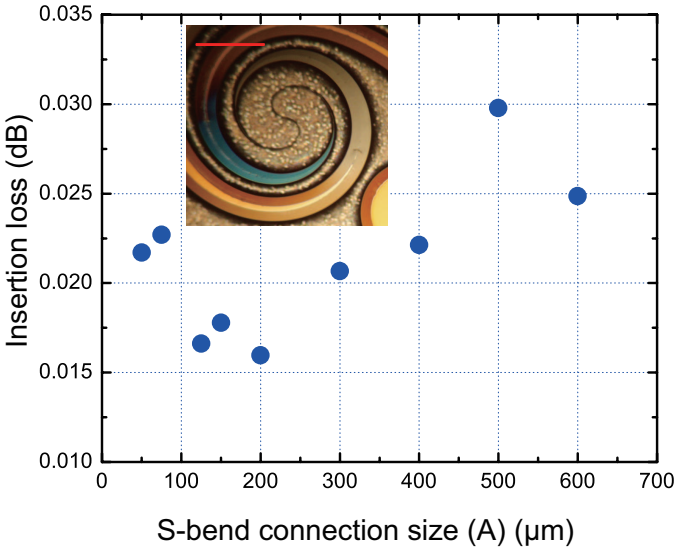

Fig. 9. Resonator-based insertion loss measurements of the S-bend connection with various size parameters (A). The inset is a microscope image of the S-bend connection with the scale bar indicating $500\,\mu m$.

Herein, the width and gap of the rectangular buffer is intentionally chosen to be $2 \times w$ and $2 \times g$ instead of w and g to avoid possible complete undercut of buffer patterns due to etching non-uniformity. At the same time, the complete undercut of the S-bend connection is desired. To achieve this goal, two buffering patterns are introduced near the S-bend connection (Fig. 1(b) and Fig. 5(a)) to reduce the loading of dry etching. We measure the undercut of the waveguide at various locations (including different places along the spirals and S-bend connection) over the entire chip ($9.5\,cm \times 9.5\,cm$). With the help of these patterns, the etching non-uniformity can be reduced to as low as $5-10\%$ across the entire chip. The uniform etching is also important to prevent the deformation or break of the structure by thermal oxide stress [11] which occurs on the oxide with excessively large undercut.

5. Conclusion

In this work, we have demonstrated the design principles and implementation of ultra-low-loss spiral waveguides. The generation of Archimedean spirals, S-bend connection, cascaded connections and input/output waveguides and buffer patterns have been presented with examples. The optical loss is carefully controlled across the entire chip. In particular for the S-Bend and the connection waveguide, adiabatic conditions are applied to minimize the transition loss by avoiding excitation of higher-order optical modes. In addition, the etching uniformity is addressed by the introduction of a buffer pattern. The design guidance provides great flexibility in creating various individual and cascaded spiral waveguide structures.

We also derived the formula for calibration of waveguide loss from backscatter measurement (previously used in [2]). The varying curvature in the spiral waveguide can impact the accuracy in the characterization of local attenuation rate. A correction term compensates this effect to provide more accurate measurement of the local attenuation rate of spiral waveguides. This correction has been previously applied in [2].

#200514 - $15.00 USD Received 5 Nov 2013; revised 27 Jan 2014; accepted 10 Feb 2014; published 27 Feb 2014

Acknowledgments
We gratefully acknowledge the Defense Advanced Research Projects Agency under the iPhoD program, the Institute for Quantum Information and Matter, an NSF Physics Frontiers Center with support of the Gordon and Betty Moore Foundation, and also the Kavli Nanoscience Institute at Caltech. H. L. thanks the Center for the Physics of Information.

#200514 - $15.00 USD Received 5 Nov 2013; revised 27 Jan 2014; accepted 10 Feb 2014; published 27 Feb 2014